
Robust Image Watermarking using Stable Diffusion

Lijun Zhang¹ Xiao Liu¹ Antoni Viros Martin² Cindy Xiong Bearfield¹ Yuriy Brun¹ Hui Guan¹

Abstract

Watermarking images is critical for tracking image provenance and claiming ownership. With the advent of generative models, such as stable diffusion, able to create fake but realistic images, watermarking has become particularly important, e.g., to make generated images reliably identifiable. Unfortunately, the very same stable diffusion technology can remove watermarks injected using existing methods. To address this problem, we present a ZoDiac, which uses a pre-trained stable diffusion model to inject a watermark into the trainable latent space, resulting in watermarks that can be reliably detected in the latent vector, even when attacked. We evaluate ZoDiac on three benchmarks, MS-COCO, DiffusionDB, and WikiArt, and find that ZoDiac is robust against state-of-the-art watermark attacks, with a watermark detection rate over 98% and a false positive rate below 6.4%, outperforming state-of-the-art watermarking methods. Our research demonstrates that stable diffusion is a promising approach to robust watermarking, able to withstand even stable-diffusion-based attacks.

1. Introduction

Digital image watermarking, a technique for subtly embedding information within digital images, has become increasingly crucial and beneficial in the context of content protection and authenticity verification (Tirkel et al., 1993; Craver et al., 1997; Boneh & Shaw, 1998; Bloom et al., 1999). The advance in generative AI technologies (Ramesh et al., 2022; Saharia et al., 2022; Rombach et al., 2022), such as stable diffusion, further underscores the need for watermarking solutions to distinguish between AI-generated and human-created images.

Much effort has been spent on embedding watermarks that

¹Manning College of Information and Computer Sciences, University of Massachusetts, Amherst MA USA ²IBM, Yorktown Heights NY USA. Correspondence to: Lijun Zhang <lijunzhang@cs.umass.edu>.

are invisible and robust to watermark removal attacks (Luo et al., 2020) in images. Conventional watermarking strategies have employed various methods, such as embedding information in texture-rich regions (Bender et al., 1996), manipulating the least significant bits (Wolfgang & Delp, 1996), or utilizing the frequency domain (Kundur & Hatzinakos, 1998). The emergence of deep learning has introduced neural network (NN)-based watermarking methods, including Convolutional Neural Network (CNN) (Zhu et al., 2018; Luo et al., 2020; Tancik et al., 2020) and Generative Adversarial Network (GAN)-based approaches (Zhang et al., 2019b;a; Huang et al., 2023). These NN-based methods have shown promise in achieving high invisibility and robustness against traditional watermarking attacks, such as adding Gaussian noise or applying JPEG compression.

Unfortunately, the recent advent of powerful image generation techniques can circumvent existing watermarking methods. The most recent work (Zhao et al., 2023a) shows that stable diffusion can be used in a watermark removal attack, and none of the existing watermarking techniques are robust enough to the attack. Figure 1 reports the watermark detection rate of existing watermarking methods after the stable-diffusion-based watermark removal attack recently proposed in (Zhao et al., 2023a). It shows the watermark detection rate drops from 79% ~ 100% before attack to only 0% ~ 29% after attack using MS-COCO dataset (Lin et al., 2014).

To address the problem, we propose a novel stable-diffusion-based watermarking framework called ZoDiac. ZoDiac uses a pre-trained stable diffusion model to inject a watermark into the trainable latent space, resulting in watermarks that can be reliably detected in the latent vector, even when at-

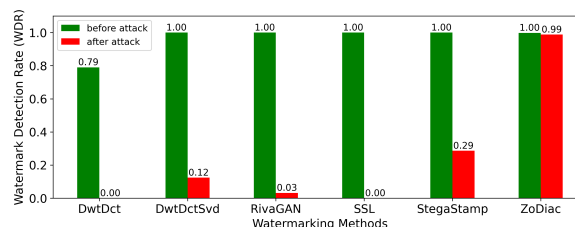


Figure 1: The watermark detection rate of existing methods and the proposed ZoDiac before and after the diffusion-based attack (Zhao et al., 2023a).

tacked. The rationale behind ZoDiac is that a pre-trained stable diffusion maps a latent vector (also called a noise vector) into an image and that *more than one latent vector can be mapped to the same image*. Given an existing image, the core idea of ZoDiac is to identify a latent vector that contains a watermark pattern and can also be mapped to the same image. ZoDiac further adaptively mixes the original image and the watermarked image, resulting in imperceptible watermarks that are highly reliable and withstand state-of-the-art watermark removal attacks. To detect watermarks, ZoDiac applies a diffusion inversion process that remaps the image to the latent vector and then detects the watermark pattern in the latent vector via a statistical test.

ZoDiac has two distinctive features. First, ZoDiac injects watermarks in the latent space that stable diffusion models operate on when sampling random noise to generate synthetic images, instead of the image space, making watermarked images both invisible and robust enough to even the most advanced stable-diffusion-based attack method (see ZoDiac in Figure 1). Second, existing watermark methods typically require the training of a dedicated model on a representative training dataset for image watermarking. In contrast, ZoDiac builds on top of pre-trained stable diffusion models, forgoing the time-consuming training process. This zero-shot capability of ZoDiac makes it applicable to any existing images.

We summarize our contributions as follows.

- *ZoDiac* — a novel framework for embedding invisible watermarks into images using pre-trained stable diffusion. To the best of our knowledge, we are the first image watermarking method that is robust to the most recent generative AI-based watermark removal attack.
- *Empirically Demonstrated Strong Robustness Against Watermark Attacks* — Our empirical evaluation on real-world images from the MS-COCO dataset (Lin et al., 2014), shows that ZoDiac is robust against the state-of-the-art watermark attack mechanism, watermark detection rate above 98% and false positive rate below 6.4%, outperforming state-of-the-art watermarking methods. Furthermore, our framework also maintains satisfying image quality with PSNR > 30dB and SSIM > 0.9 (two methods of measuring similarity with the unwatermarked image), underscoring its efficacy in achieving robust watermarking with quality preservation.
- *Robustness Against Combined Attacks* — Prior watermarking method evaluations (Wen et al., 2023; Zhao et al., 2023a) focused on robustness to only a single attack at a time. We show that in a more realistic scenario, where the attacker can combine multiple attacks, ZoDiac significantly outperforms all existing methods. For example, when combining all attacks other than

image rotation, ZoDiac retains a detection rate above 50% while all existing methods fail with a detection rate of 0%. None of the existing methods (except SSL (Fernandez et al., 2022)) are effective against rotation (while SSL is not effective against some other attacks). We propose a method for making ZoDiac robust to rotation (above 99%), only slightly increasing its false-positive rate (from 0.4% to 3.4%).

2. Preliminary

This section first introduces the image watermarking problem and then the background of the diffusion model necessary to follow the ZoDiac framework.

2.1. Robust Image Watermarking Problem

The objective of image watermarking is to embed a pre-defined watermark into a given input image. This process aims to ensure that the watermarked image retains visual similarity to the original image. This similarity can be quantified using metrics such as the Peak Signal-to-Noise Ratio (PSNR), the Structural Similarity Index (SSIM) (Wang et al., 2004), and the Learned Perceptual Image Patch Similarity (LPIPS) (Zhang et al., 2018). Furthermore, the watermarked image should be robust to malicious attacks that aim to remove the watermarks. Those attacks will not change the image content a lot but may be able to remove the watermark. A robust image watermarking method should be resistant to different types of attacks.

2.2. Diffusion Models and DDIM Inversion

Diffusion probabilistic models (Sohl-Dickstein et al., 2015) evolve from the forward diffusion process, where a data point sampled from a real data distribution $x_0 \sim q(x)$ is gradually converted into a noisy representation x_T through T steps of progressive Gaussian noise addition. This transformation yields x_T as an isotropic Gaussian noise, i.e., $x_T \sim \mathcal{N}(\mathbf{0}, \mathbf{I})$. Specifically, the transformation follows the Markov Chain,

$$q(x_t|x_{t-1}) = \mathcal{N}(x_t; \sqrt{1 - \beta_t}x_{t-1}, \beta_t\mathbf{I}), \quad (1)$$

where $\beta_t \in (0, 1)$ is the scheduled noise variance that controls the step size. A direct generation of x_t from x_0 can be expressed by

$$x_t = \sqrt{\bar{\alpha}_t}x_0 + \sqrt{1 - \bar{\alpha}_t}\epsilon, \quad (2)$$

where $\bar{\alpha}_t = \prod_{i=0}^{t-1} (1 - \beta_i)$ and $\epsilon \sim \mathcal{N}(0, \mathbf{I})$.

The diffusion models aim to reverse this forward process, learning to retrieve the original image x_0 from the noise x_T by estimating the noise at each step and iteratively performing denoising. The Denoising Diffusion Implicit Model

(DDIM) (Song et al., 2020) is a prominent denoising method within this context, known for its efficiency and deterministic output. It requires fewer steps, sometimes only 50, to replicate the denoising achieved by the standard 1000-step process, and consistently reproduces x_0 from a given x_T , providing deterministic reconstruction. Formally, for each denoising step t , a learned noise predictor ϵ_θ estimates the noise $\epsilon_\theta(x_t)$ added to x_0 , leading to the estimation of x_0 as follows:

$$x'_0 = \frac{x_t - \sqrt{1 - \bar{\alpha}_t} \epsilon_\theta(x_t)}{\sqrt{\bar{\alpha}_t}}. \quad (3)$$

Then the estimated noise $\epsilon_\theta(x_t)$ is reintroduced to the approximated x'_0 to determine x_{t-1} , without the addition of extra noise yielding:

$$x_{t-1} = \sqrt{\bar{\alpha}_{t-1}} x'_0 + \sqrt{1 - \bar{\alpha}_{t-1}} \epsilon_\theta(x_t). \quad (4)$$

In this way, we could deterministically recover the same x_0 from the specified x_T and DDIM permits the omission of some intermediate steps according to the noise schedule.

DDIM also enables an inversion mechanism (Dhariwal & Nichol, 2021), allowing for a reconstruction of the noise representation x_T from an image x_0 . The retrieved x_T should be able to be remapped to an image close to x_0 through DDIM. The DDIM inversion is modeled as:

$$\hat{x}_t = \sqrt{\bar{\alpha}_t} x_0 + \sqrt{1 - \bar{\alpha}_t} \epsilon_\theta(x_{t-1}). \quad (5)$$

In essence, DDIM inversion adheres to the forward diffusion process in Equation 2, substituting ϵ_t with $\epsilon_\theta(x_t)$ at each timestep. We denote the denoising process, that is, the image generation process as \mathcal{G} and its inversion as \mathcal{G}' .

Notice that in stable diffusion model (Rombach et al., 2022), the image generation are performed on the latent vector representation \mathbf{Z}_T , of the noise x_T . We refer to \mathbf{Z}_T as the *latent vector*. The transformation between the image and the latent vector is carried out with a pre-trained Variational Autoencoder (VAE).

3. Proposed Framework: ZoDiac

This section introduces ZoDiac, a novel zero-shot watermarking technique that leverages the capabilities of pre-trained stable diffusion models. ZoDiac is designed to embed watermarks into images such that the resulting watermarked images remain visually similar to the original, while also being robust against watermark removal attacks. The foundation of our approach lies in learning a latent vector that encodes a pre-defined watermark within its Fourier space, and can be mapped by pre-trained stable diffusion models into an image closely resembling the original.

3.1. Overview of ZoDiac

Figure 2 illustrates the ZoDiac framework. ZoDiac consists of three main steps, *latent vector initialization*, *watermark encoding*, and *adaptive image enhancement*, to embed a watermark in an existing image and one step, *watermark decoding*, to detect the embedded watermark. We first explain the high-level idea of each step and then their details in § 3.2-3.5.

Algorithm 1 lists the pseudocode of the watermark generation phase in ZoDiac. The original image x_0 first undergoes a DDIM inversion process to identify its latent vector representation \mathbf{Z}_T (1. Latent Vector Initialization, Line 1). ZoDiac then encodes a watermark in the latent vector \mathbf{Z}_T and trains the watermarked latent vector such that a pre-trained stable diffusion model can use it to generate a watermarked image similar to the original image (2. Watermark Encoding, Lines 2-5). To encode the watermark into \mathbf{Z}_T , \mathbf{Z}_T is converted to its Fourier space, encoded with a given watermark \mathbf{W} , and then transformed back to the spatial domain prior to being fed into the diffusion model. ZoDiac preserves the visual similarity between the generated image \hat{x}_0 and the original image x_0 by optimizing the latent vector via a carefully designed reconstruction loss. The diffusion model remains frozen and operates in inference mode during the optimization, making it converge very fast. The gradient flow during backpropagation is indicated by the dashed red arrows in Figure 2. After image generation, ZoDiac mixes the watermarked image \hat{x}_0 with the original one x_0 to further enhance image quality (3. Adaptive Image Enhancement, Lines 6-7).

In the detection phase, ZoDiac first reconstructs the latent vector of the image under inspection via DDIM inversion, transforms the latent vector into the Fourier space, and then conducts a statistical test for watermark detection (4. Watermark Decoding).

Algorithm 1 ZoDiac-Watermarking

Require: original image x_0 , watermark \mathbf{W}

Require: pre-trained diffusion model \mathcal{G} , and its inversion \mathcal{G}'

Require: diffusion steps T , latent update steps N

Require: SSIM threshold s^*

Ensure: watermarked image \bar{x}_0

1: $\mathbf{Z}_T \leftarrow \mathcal{G}'(x_0)$

2: **for** $i = 1$ to N **do**

3: $\hat{x}_0 \leftarrow \mathcal{G}(\mathbf{Z}_T \oplus \mathbf{W})$

4: Take gradient descent on $\nabla_{\mathbf{Z}_T} \mathcal{L}(x_0, \hat{x}_0)$ {Eq. 9}

5: **end for**

6: Search $\gamma^* \in [0, 1]$ s.t. $S(\bar{x}_0, x_0) \geq s^*$ {Eq. 11}

7: $\bar{x}_0 = \hat{x}_0 + \gamma^*(x_0 - \hat{x}_0)$ {Eq. 10}

8: **return** \bar{x}_0

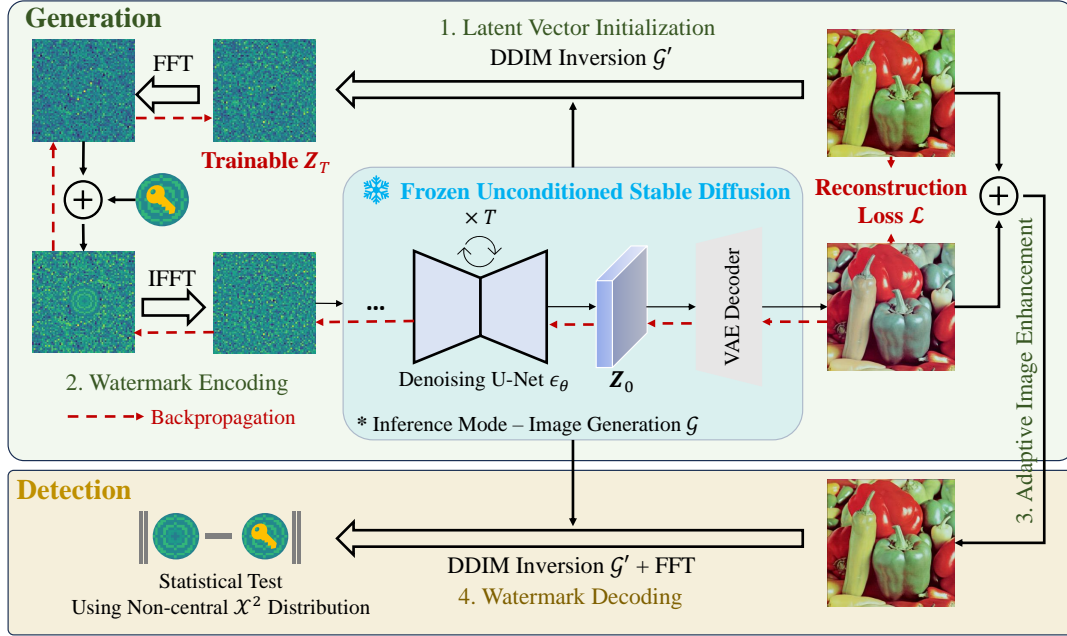


Figure 2: Overview of ZoDiac with watermarked image generation and detection. There are three major steps in the generation phase: 1) latent vector initialization, 2) watermark encoding, and 3) adaptive image enhancement. In the detection phase, the watermark is decoded by performing DDIM inversion, Fourier transformation, and statistical testing.

3.2. Latent Vector Initialization

Finding a good initialization for the latent vector \mathbf{Z}_T is critical to reduce the time spent on optimizing the latent vector. Latent vector initialization initializes the trainable latent vector in a way that the stable diffusion model can reproduce the original image x_0 with it. Specifically, ZoDiac employs DDIM inversion to generate the initial latent vector $\mathbf{Z}_T = \mathcal{G}'(x_0)$ that can be effectively remapped to the original image via DDIM.

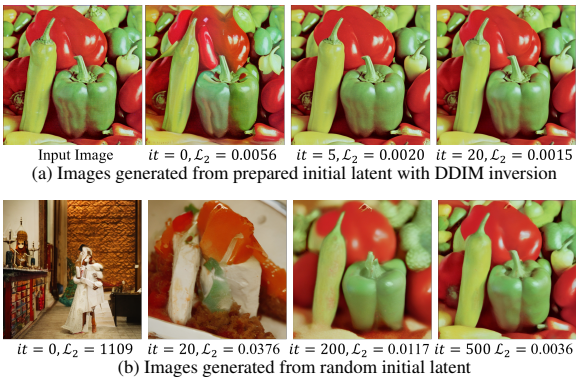


Figure 3: Watermarked images along with the optimization iterations and \mathcal{L}_2 loss values. We observe much faster convergence when (a) using the latent vector initialized from the DDIM inversion compared to (b) using a randomly initialized latent vector.

Figure 3 compares the watermarked images at different optimization iterations when training the latent vector initialized with the vector from DDIM inversion (a) and a vector randomly sampled from the Gaussian distribution (b). The optimization happens after a watermark is encoded into the initialized latent vector and will be detailed in § 3.3. The result shows the advantage of the latent vector initialization step, which achieves a higher quality image, measured by the \mathcal{L}_2 distance between the image and its original counterpart with only 20 iterations. In contrast, a randomly initialized latent vector requires more than hundreds of iterations to produce a similar image whose quality ($\mathcal{L}_2 = 0.0036$) still largely falls behind.

3.3. Watermark Encoding

The watermark encoding step aims to encode a watermark into an image with minimal impact on its visual quality. It first injects the watermark into the Fourier Space of the latent vector of an image and then optimizes the watermarked latent vector to ensure that it can be used to synthesize an image resembling the original one. Our fundamental assumptions are two-folds: (1) injecting watermarks into the latent space of images can effectively counter watermark removal attacks operated at the image space; (2) injecting watermarks into the Fourier representation of a latent vector helps preserve the quality of the watermarked image.

Watermark Injection. ZoDiac injects a concentric ring-

like watermark into the Fourier space of a latent vector, leading to a circularly symmetric watermark embedding in the low-frequency domain, which is proved to be resistant to geometric transformations and common image distortions (Solachidis & Pitas, 2001). A recent work (Wen et al., 2023) also adopts this ring-like watermark pattern but it focuses on watermarking stable diffusion models instead of existing images. We next describe how to construct a watermark and how to embed the watermark.

ZoDiac assumes that elements in a watermark \mathbf{W} are generated by randomly sampling from a complex Gaussian distribution, noted as $\mathcal{CN}(0, 1)$. Elements in the watermark that are of the same distance to the center of the latent vector have the same value, making it a so-called ‘‘ring-like’’ watermark. Mathematically, let $\mathcal{F}(\mathbf{Z}_T) \in \mathbb{C}^{ch \times w \times h}$ be the Fourier transformed latent vector, where ch is the number of channels, w and h are the width and height. Let $p = (i, j)$ be a coordinate, $c = (h/2, w/2)$ be the latent vector’s center, and $d(p, c)$ be the Euclidean distance from a coordinate to the center. Each element in the watermark $\mathbf{W} \in \mathbb{R}^{w \times h}$ is:

$$\mathbf{W}_p = w_{\lceil d(p,c) \rceil}, \quad \text{where } w_{\lceil d(p,c) \rceil} \sim \mathcal{CN}(0,1). \quad (6)$$

To embed the watermark \mathbf{W} into the Fourier representation of the latent vector $\mathcal{F}(\mathbf{Z}_T)$, we also need a binary mask that indicates the location where the watermark will be applied. Mathematically, let $\mathbf{M} \in \{0, 1\}^{w \times h}$ be a binary circular mask with a predefined radius d^* . Each item in the mask \mathbf{M} is

$$\mathbf{M}_p = \begin{cases} 1, & \text{if } d(p, c) \leq d^*; \\ 0, & \text{otherwise.} \end{cases} \quad (7)$$

Finally the watermark \mathbf{W} is applied to the Fourier-transformed latent vector $\mathcal{F}(\mathbf{Z}_T)$ with the binary mask \mathbf{M} , $\mathcal{F}(\mathbf{Z}_T)[-1, :, :] = (1 - \mathbf{M}) \odot \mathcal{F}(\mathbf{Z}_T)[-1, :, :] + \mathbf{M} \odot \mathbf{W}$, (8)

where \odot denotes the element-wise product. We inject the watermark into the last channel of $\mathcal{F}(\mathbf{Z}_T)$ as it causes the least influence on the generated image quality. We denote the latent vector after watermarking as $\mathbf{Z}_T \oplus \mathbf{W}$.

Latent Vector Optimization. ZoDiac then seeks to find a latent vector \mathbf{Z}_T such that, when being watermarked by \mathbf{W} and then processed by the denoising process \mathcal{G} , generates an image \hat{x}_0 that is the most similar to the original image x_0 . To solve the optimization problem, we design a reconstruction loss \mathcal{L} that allows ZoDiac to iteratively refine \mathbf{Z}_T via standard backpropagation:

$$\mathcal{L} = \mathcal{L}_2(x_0, \hat{x}_0) + \lambda_s \mathcal{L}_s(x_0, \hat{x}_0) + \lambda_p \mathcal{L}_p(x_0, \hat{x}_0), \quad (9)$$

where $\hat{x}_0 = \mathcal{G}(\mathbf{Z}_T \oplus \mathbf{W})$, \mathcal{L}_2 is the Euclidean distance, \mathcal{L}_s represents the SSIM loss (Zhao et al., 2016), \mathcal{L}_p corresponds to the Watson-VGG perceptual loss (Czolbe et al.,

2020), and λ_s, λ_p are their respective weighting coefficients. These coefficients are set to balance the scale of each loss component.

3.4. Adaptive Image Enhancement

Adaptive image enhancement aims to improve the visual quality of the image \hat{x}_0 from the watermark encoding step. It achieves the goal by adaptively mixing \hat{x}_0 with the original image x_0 such that the *mixed image* can meet a desired image quality threshold. Mathematically, the mixed image \bar{x}_0 is formulated as follows.

$$\bar{x}_0 = \hat{x}_0 + \gamma(x_0 - \hat{x}_0), \quad (10)$$

where $\gamma \in [0, 1]$ is a modulating factor. A higher γ improves image quality at the cost of potential watermark diminishing. Adaptive image enhancement automatically identifies the smallest γ that results in desired image quality through binary search. It optimizes the following objective:

$$\min \gamma, \quad \text{s.t. } S(\bar{x}_0, x_0) \geq s^*, \quad (11)$$

where s^* is the desired image quality and S is an image similarity metric. In this paper, we use the SSIM metric by default.

3.5. Watermark Decoding

In the watermark detection phase, our primary objective is to verify whether a given image x_0 contains the embedded watermark \mathbf{W} . The detection process starts with transforming x_0 to $\mathbf{y} = \mathcal{F}(\mathcal{G}'(x_0))[-1, :, :] \in \mathbb{C}^{w \times h}$, representing the last channel of the Fourier representation of the latent vector. It then detects the presence of \mathbf{W} in \mathbf{y} via a statistical test procedure. The statistical test computes a P-value, an interpretable statistical metric that quantifies the likelihood of the observed watermark manifesting in a natural image by random chance. A watermark is considered detected when the computed P-value falls below a chosen threshold.

To compute the P-value, we first define a null hypothesis and then validate the hypothesis. The DDIM inversion \mathcal{G}' maps any test image x_0 into a Gaussian distribution, following the forward diffusion process (Sohl-Dickstein et al., 2015). As the Fourier transformation of a Gaussian distribution remains Gaussian, we define the following null hypothesis:

$$\mathbf{H}_0 : \mathbf{y} \sim \mathcal{N}(\mathbf{0}, \sigma^2, \mathbf{I}_C). \quad (12)$$

Here, σ^2 is estimated for each image from the variance of \mathbf{y} masked by the circular binary mask \mathbf{M} , i.e., $\sigma^2 = \frac{1}{\sum \mathbf{M}} \sum (\mathbf{M} \odot \mathbf{y})^2$.

To validate this hypothesis, we define a distance score η that measures the disparity between \mathbf{W} and \mathbf{y} in the area defined by the binary mask \mathbf{M} :

$$\eta = \frac{1}{\sigma^2} \sum (\mathbf{M} \odot \mathbf{W} - \mathbf{M} \odot \mathbf{y})^2. \quad (13)$$

Under H_0 , η follows a non-central chi-squared distribution (Patnaik, 1949), characterized by $\sum \mathbf{M}$ degrees of freedom and a non-centrality parameter $\lambda = \frac{1}{\sigma^2} \sum (\mathbf{M} \odot \mathbf{W})^2$. An image is classified as watermarked if the value of η is statistically improbable under random conditions. The probability p of observing a value as extreme as η is derived from the cumulative distribution function of the non-central chi-squared distribution.

Therefore, non-watermarked images will exhibit higher P-values, while watermarked images yield lower values, indicating a successful rejection of H_0 and confirming the watermark’s presence. In practice, we treat $1-P$ -value as the likelihood of watermark presence and set up a detection threshold p^* to determine its presence. An image with $1-P$ -value above p^* is considered to be watermarked. More explorations on p^* are provided in the Appendix.

4. Experiments

This section evaluates the efficacy of the ZoDiac framework using a diverse domain of images including real photographs, AI-generated content, and visual artwork.

4.1. Experimental Settings

Datasets. We utilizes three distinct datasets:

- **Real Photos:** 500 images are randomly selected from the MS-COCO dataset (Lin et al., 2014), a large-scale image dataset containing over 328K captioned images.
- **AI-Generated Images:** For content produced by AI systems, 500 images are randomly chosen from **DiffusionDB** (Wang et al., 2022). This dataset comprises images generated by Stable Diffusion, based on prompts and hyperparameters from actual user interactions.
- **Visual Arts:** 500 images are sampled from the **WikiArt** dataset (Phillips & Mackintosh, 2011), which includes different art pieces sourced from WikiArt.org.

ZoDiac Settings. We utilize the pre-trained stable diffusion model *stable-diffusion-2-1-base* (Rombach et al., 2022) with 50 denoising steps for image generation. The optimization of the trainable latent variable is conducted over 100 iterations using the Adam optimizer (Kingma & Ba, 2014). The weights for the SSIM loss λ_s and the perceptual loss λ_p are carefully calibrated to 0.1 and 0.01, respectively, in order to balance the scales of the various loss components. Following Tree-Rings (Wen et al., 2023), we set the watermark radius d^* to 10. To determine the quality and detectability of the watermark, we set the SSIM threshold s^* to 0.92 and the detection threshold p^* to 0.9 unless noted differently. Evaluations with other hyperparameter settings are presented in the ablation study (§ 4.3) and the Appendix.

Watermarking Baselines. We compare ZoDiac with five

invisible watermarking methods.

- **Traditional Methods:** We include two conventional techniques, **DwtDct** and **DwtDctSvd** (Cox et al., 2007), which utilize frequency decomposition. As a classic and powerful watermarking method, DwtDctSvd is employed to watermark stable diffusion models in (Rombach et al., 2022).
- **Training-Based Methods:** Our comparison also extends to three advanced training-based approaches. **Ri-vaGAN** (Zhang et al., 2019b) is a pre-trained GAN-based model incorporating an attention mechanism. **StegaStamp** (Tancik et al., 2020) applies adversarial training and integrates both convolutional neural network (CNN) and spatial transformer techniques. Finally, **SSL** (Fernandez et al., 2022) represents a latent space-based watermarking method, utilizing self-supervised learning for network pretraining.

Watermark Attack Methods. To evaluate the robustness of ZoDiac, we test it against a comprehensive set of watermarking attacks. These attacks represent a spectrum of common image perturbations and manipulations. The set of attacks employed in our testing includes:

- Adjustments in brightness or contrast with a factor of 0.5.
- JPEG compression with a quality setting of 50.
- Image rotation by 90 degrees.
- Addition of Gaussian noise with a std of 0.05.
- Gaussian blur with kernel size of 5 and std of 1.
- BM3D denoising algorithm with a std of 0.1.
- Two Variational AutoEncoder (VAE) based image compression models, *Bmshj18* (Ballé et al., 2018) and *Cheng20* (Cheng et al., 2020), both with compression factors of 3.
- A stable diffusion-based image regeneration model, *Zhao23* (Zhao et al., 2023a) with 60 denoising steps.

We also conducted tests with a composite attack that combines all the aforementioned individual attacks named *All* and a variant without rotation named *All w/o Rotation*. These manipulations represent effective image-processing operations that could potentially interfere with watermarks.

Evaluation Metrics. We evaluate the quality of the watermarked images compared to the original image using three metrics: Peak Signal-to-Noise Ratio (PSNR) defined as $PSNR(x, \bar{x}) = -10 \cdot \log_{10}(MSE(x, \bar{x}))$, Structural Similarity Index (SSIM) (Wang et al., 2004) with range $[0, 1]$, and LPIPS (Zhang et al., 2018) which measures perceptual similarity. PSNR and SSIM are higher the better image quality, while LPIPS is lower the more similar. To assess watermark robustness, we quantify the average Watermark Detection Rate (WDR) over watermarked images, both pre-attack and post-attack. We also report WDR for non-watermarked images, which is called the False Positive

Rate (FPR). Both WDR and FPR range from 0 to 1. We expect to achieve high WDR and low FPR.

4.2. Results

Table 4 reports the quality of watermarked images and the watermark detection rate before and after attacks for ZoDiac and the baselines on the MS-COCO, DiffusionDB, and WikiArt datasets.

Image Quality. ZoDiac achieves satisfying perceptual similarity, approximately 30dB in PSNR and 0.92 in SSIM (Chatterjee et al., 2020; Subhedar & Mankar, 2020). Notably, its image quality outperforms the most robust watermarking method, StegaStamp (also see black stains shown in Figure 5). Increasing the SSIM threshold can further improve image quality with a compromise in watermark detection rate, as stated in § 3.4. The trade-offs are further examined in § 4.3

Watermark Robustness. ZoDiac consistently exhibits high detection rates, exceeding 0.98, against watermark removal algorithms as highlighted by the gray cells (*Rotation* being an exception). Traditional approaches such as DwtDct and DwtDctSvd consistently fail to brightness and contrast changes, rotation, and advanced generated AI-based attacks. RivaGAN and SSL are susceptible to advanced attacks, *Bmshj18*, *Cheng20*, and *Zhao23*. StegaStamp, despite being robust across most attacks, fails under rotation and demonstrates significantly diminished detection rates under *Zhao23*, the diffusion model-based attack.

The exception of rotation is noteworthy. All methods, apart from SSL which incorporates rotation during training, do not sustain their watermark under rotational disturbances. This limitation in ZoDiac stems from the non-rotation-invariant nature of the DDIM inversion process; the latent representation derived from an image and its rotated version differ significantly. However, rotation does not constitute an invisible attack, and its effects are readily reversible, allowing users to manually correct image orientation to facilitate watermark detection. An extended discussion on handling rotational attacks is presented in § 4.4.

When facing the composite attack excluding rotation (see the *All w/o Rotation* column), ZoDiac maintains a reasonable detection rate of around 0.5. In contrast, all baselines fail to withstand such a sophisticated attack with a WDR close to zero.

4.3. Ablation Study

This section reports the impact of two key hyperparameters, the SSIM threshold s^* and the detection threshold p^* , on the quality of watermarked images and watermark robustness. It also validates the consistent performance of ZoDiac with different stable diffusion backbones.

Varying the SSIM Threshold s^* . As stated in § 3.4, while a high image quality threshold s^* can yield an image with negligible quality loss, it conversely raises the risk of watermark elimination. In this study, we explore the impact of varying s^* values on the trade-off between image quality and watermark robustness. Figure 6 illustrates the trade-off curves on the MS-COCO dataset, subject to various attack methods. It shows the watermarked image quality in SSIM (x-axis) against the watermark detection rate (y-axis), in which ZoDiac’s image quality is adjusted by SSIM thresholds $s^* \in [0.8, 0.98]$ with a step size of 0.03. Results for the DiffusionDB and WikiArt datasets are included in the Appendix.

We made two main observations. First, ZoDiac demonstrates watermark robustness that is on par with, or surpasses, that of the baseline methods under similar image quality. For instance, when brightness or contrast changes, ZoDiac’s WDR approximates that of RivaGAN and SSL. Notably, against more advanced watermark removal techniques, as depicted in the final row, ZoDiac consistently outperforms all baseline methods in terms of robustness. Second, although the adaptive image enhancement step can also enhance the watermarked image quality of StegaStamp, the most robust baseline method, it causes a significant decline in its watermark robustness, as shown by the pink line in Figure 6. It is because StegaStamp injects watermarks in the image space, making it more sensitive to the enhancement. In contrast, ZoDiac injects watermarks in the latent space of images, allowing it to benefit from the enhancement step in achieving a balance between good image quality and high watermark robustness.

Varying the Detection Threshold p^* . An image is identified as watermarked if its 1-P-value exceeds the detection threshold p^* as introduced in § 3.5. A larger p^* imposes a stricter criterion for watermark recognition, reducing both the probability of watermark detection for watermarked images, measured by watermark detection rate (WDR), and false identification for non-watermarked images, measured by false positive rate (FPR). Table 7 reports the effects of detection thresholds $p^* \in \{0.90, 0.95, 0.99\}$ on WDR and FPR. WDR is evaluated on watermarked images generated with SSIM threshold $s^* = 0.92$. Results for pre-attack and post-attack under three representative attacks, *Rotation*, *Zhao23*, and *All w/o Rotation* are provided and the full table under all attacks is included in the Appendix. Table 7 confirms the anticipated relationship between WDR and FPR with respect to the detection threshold: a higher p^* corresponds to lower rates of both WDR and FPR. The result suggests a detection threshold of $p^* = 0.9$ to maintain a high WDR while ensuring an acceptable FPR in practice.

Varying the Backbone Models. ZoDiac is compatible with different versions of pre-trained stable diffusion models. In

Table 4: Image quality in terms of PSNR, SSIM, and LPIPS, and watermark robustness in terms of Watermark Detection Rate (WDR) before and after attacks, on **MS-COCO**, **DiffusionDB**, and **WikiArt** datasets. The watermark detection rates above 0.98 are highlighted by gray cells.

Watermarking Method	Image Quality			Watermark Detection Rate (WDR) \uparrow before and after Attack												
	PSNR \uparrow	SSIM \uparrow	LPIPS \downarrow	Pre-Attack	Post-Attack										All	All w/o Rotation
					Brightness	Contrast	JPEG	Rotation	G-Noise	G-Blur	BM3D	Bmshj18	Cheng20	Zhao23		
COCO																
DwtDct	37.88	0.97	0.02	0.790	0.000	0.000	0.000	0.000	0.687	0.156	0.000	0.000	0.000	0.000	0.000	0.000
DwtDctSvd	38.06	0.98	0.02	1.000	0.098	0.100	0.746	0.000	0.998	1.000	0.452	0.016	0.032	0.124	0.000	0.000
RivaGAN	40.57	0.98	0.04	1.000	0.996	0.998	0.984	0.000	1.000	1.000	0.974	0.010	0.010	0.032	0.000	0.000
SSL	41.81	0.98	0.06	1.000	0.992	0.996	0.046	0.952	0.038	1.000	0.000	0.000	0.000	0.000	0.000	0.000
StegaStamp	28.64	0.91	0.13	1.000	0.998	0.998	1.000	0.000	0.998	1.000	0.998	0.998	1.000	0.286	0.000	0.002
ours	29.41	0.92	0.09	0.998	0.998	0.998	0.992	0.538	0.996	0.996	0.994	0.992	0.986	0.988	0.072	0.510
DiffusionDB																
DwtDct	37.77	0.96	0.02	0.690	0.000	0.000	0.000	0.000	0.574	0.224	0.000	0.000	0.000	0.000	0.000	0.000
DwtDctSvd	37.84	0.97	0.02	0.998	0.088	0.088	0.812	0.000	0.982	0.996	0.686	0.014	0.030	0.116	0.000	0.000
RivaGAN	40.60	0.98	0.04	0.974	0.932	0.932	0.898	0.000	0.958	0.966	0.858	0.008	0.004	0.024	0.000	0.000
SSL	41.84	0.98	0.06	0.998	0.990	0.996	0.040	0.898	0.030	1.000	0.000	0.000	0.000	0.000	0.000	0.000
StegaStamp	28.51	0.90	0.13	1.000	0.998	0.998	1.000	0.000	0.998	0.998	1.000	0.996	0.998	0.302	0.000	0.002
ours	29.18	0.92	0.07	1.000	0.998	0.998	0.994	0.558	0.998	1.000	1.000	0.994	0.992	0.988	0.086	0.548
WikiArt																
DwtDct	38.84	0.97	0.02	0.754	0.000	0.000	0.000	0.000	0.594	0.280	0.000	0.000	0.000	0.000	0.000	0.000
DwtDctSvd	39.14	0.98	0.02	1.000	0.096	0.094	0.698	0.000	1.000	1.000	0.668	0.034	0.072	0.116	0.000	0.000
RivaGAN	40.44	0.98	0.05	1.000	0.998	1.000	0.990	0.000	1.000	1.000	0.992	0.010	0.024	0.024	0.000	0.000
SSL	41.81	0.99	0.06	1.000	0.988	0.988	0.082	0.932	0.108	1.000	0.000	0.000	0.000	0.000	0.000	0.000
StegaStamp	28.45	0.91	0.14	1.000	1.000	0.998	1.000	0.000	1.000	1.000	1.000	1.000	1.000	0.182	0.000	0.002
ours	30.04	0.92	0.10	1.000	1.000	1.000	1.000	0.478	0.998	1.000	1.000	0.994	0.994	0.992	0.082	0.530

this study, we extend our evaluations to the *stable-diffusion-v1-4* model, in addition to the previously utilized *stable-diffusion-2-1-base*. Figure 8 shows the trade-off curves between the watermarked image quality and the watermark detection rate without attack as well as with three representative attacks, *Rotation*, *Zhao23*, and *All w/o Rotation*. Additional results addressing other attack types are included in the Appendix. The figure shows a consistent performance (i.e., WDR and image quality in SSIM) between the two evaluated pre-trained models, as indicated by the almost overlapped solid and dashed lines. It suggests that ZoDiac can seamlessly integrate with any pre-trained stable diffusion model, maintaining its state-of-the-art efficiency, regardless of the backbone model employed.

4.4. Discussion on Rotation Attack

The rotation attack presents a significant challenge for most existing watermarking methods, including ZoDiac, as shown in Table 4. There are two potential strategies to mitigate this issue. The first approach, exemplified by SSL, integrates rotation into the model’s training phase as a type of data augmentation. However, this method is incompatible with the zero-shot nature of ZoDiac. The second approach, as mentioned in § 4.2, involves rectifying the image’s orientation prior to watermark detection. This correction can be achieved manually or via an automated process. For the latter, one can systematically rotate the image through a series of predetermined angles, spanning the full 360-degree spectrum, and perform watermark detection at each increment. We call the defense “rotation auto-correction”.

In this study, we test “rotation auto-correction” in improving the performance of ZoDiac. We conduct experiments using intervals of 5, 10, and 30 degrees and report the corresponding Watermark Detection Rate (WDR) for watermarked images subjected to the 90-degree rotation attack, as well as the False Positive Rates (FPR) for unmarked images. Table 9 reports the results on the MS-COCO dataset with the SSIM threshold s^* fixed at 0.92.

As expected, applying rotation auto-correction enables ZoDiac to achieve a higher WDR. However, it also increases the risk of detecting a watermark from the unmarked images, leading to a higher FPR. When we set up a higher detection threshold $p^* = 0.99$, the increased FPR can be greatly suppressed with a slight decrease in WDR. Therefore in practice, if we employ the “rotation auto-correction” defense, it is reasonable to set a higher detection threshold than $p^* = 0.9$.

5. Related Work

Digital Image Watermarking. Digital watermarking, particularly in the image domain, has been a cornerstone in computer vision for decades. Traditional methods have predominantly relied on frequency decomposition techniques such as Discrete Fourier Transform (DFT) (Urvoy et al., 2014), Discrete Cosine Transform (DCT) (Bors & Pitas, 1996), Discrete Wavelet Transform (DWT) (Xia et al., 1998), or their combinations (Cox et al., 2007). These frequency-based methods are advantageous due to their inherent resilience to common image manipulations, including translations, rotations, and resizing, facilitating the creation of

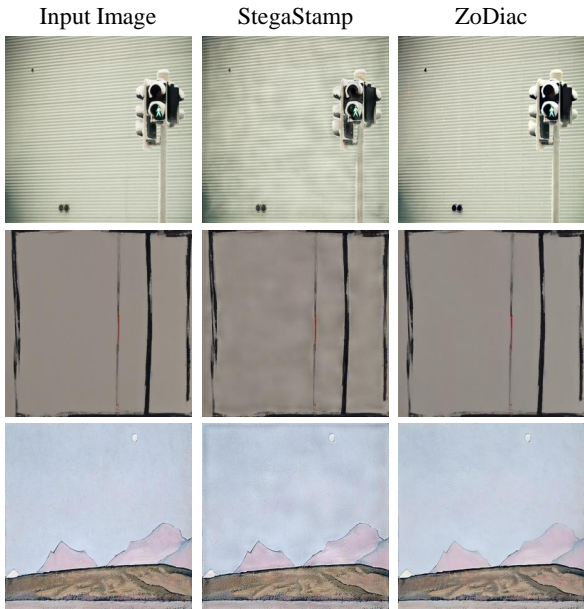


Figure 5: Watermarked images generated from StegaStamp and ZoDiac.

watermarks robust to such transformations.

The development of deep neural networks (DNN) has introduced novel learning-based watermarking approaches. HiD-DeN (Zhu et al., 2018) employs joint training of watermark encoder and decoder alongside noise layers that mimic image perturbations. It leverages an adversarial discriminator for enhanced visual quality and has been expanded for arbitrary image resolutions and message lengths in (Lee et al., 2020). Regarding the watermark robustness, StegaStamp (Tancik et al., 2020) uses differentiable image perturbations during training to improve noise resistance and incorporates a spatial transformer network for minor perspective and geometric changes. Distortion Agnostic (Luo et al., 2020) further brings robustness to unforeseen transformations by introducing adversarial training. Considering the watermarking as an image generation process, RivaGAN (Zhang et al., 2019b), SteganoGAN (Zhang et al., 2019a), and ARWGAN (Huang et al., 2023) resort to generative AI, particularly Generative Adversarial Network (GAN), for enhanced performance and robustness in watermarking. A comprehensive review is provided in (Wan et al., 2022). With the demonstrated efficacy of diffusion models in image generation (Dhariwal & Nichol, 2021), our work pioneers the use of pre-trained diffusion models for zero-shot robust image watermarking.

Diffusion Model Watermarking. Rapid evolution in deep generative models has led to methods capable of synthesizing high-quality, realistic images (Dhariwal & Nichol, 2021). These models pose threats to society due to their

potential misuse, prompting the necessity to differentiate AI-generated images from those created by humans. Recent efforts resort to watermarking the model itself, which focuses on enabling these models to automatically generate watermarked images for easier identification later. One straightforward approach is to fine-tune diffusion models with datasets containing watermarked images, leading these models to inherently produce watermarked outputs (Cui et al., 2023; Wang et al., 2023; Zhao et al., 2023b; Zeng et al., 2023). Alternatives like Stable Signature (Fernandez et al., 2023) focus on training a dedicated watermark decoder to fine-tune only the latent decoder part of the stable diffusion model. Tree-Rings (Wen et al., 2023) takes a different route by embedding watermarks in the initial noise latent, detectable through DDIM inversion (Dhariwal & Nichol, 2021). Although these methods effectively lead diffusion models to generate watermarked images, they are not equipped for watermarking existing images, a functionality our approach is designed to provide.

Image Watermarking Attack. Watermarking attacks are typically categorized into two types (Zhao et al., 2023a). Destructive attacks treat the watermark as part of the image, seeking to remove it through image corruption. Common methods include altering image brightness or contrast, applying JPEG compression, introducing Gaussian noise, and so on. Constructive attacks, on the other hand, view the watermark as noise superimposed on the original image, focusing on its removal via image purification techniques such as Gaussian blur (Hosam, 2019), BM3D (Dabov et al., 2007), and learning-based methods like DnCNNs (Zhang et al., 2017). Recently, regeneration attacks have emerged, leveraging the strengths of both destructive and constructive approaches. These attacks corrupt the image by adding Gaussian noise to its latent representation, then reconstruct it using generative models such as Variational AutoEncoders (Ballé et al., 2018; Cheng et al., 2020) or Stable Diffusion (Rombach et al., 2022). We aim to effectively counter all types of attacks when watermarking given images.

6. Conclusion

This paper introduced ZoDiac, a zero-shot diffusion model-based watermarking framework. The key to our method lies in its ability to hide watermarks within the trainable latent space of a pre-trained stable diffusion model, thereby enhancing the watermark robustness while preserving the perceptual quality of the watermarked images. Extensive evaluations across various datasets, including MS-COCO, DiffusionDB, and WikiArt, have demonstrated ZoDiac’s effectiveness in achieving both invisibility and robustness to various watermark removal attacks, especially advanced generative AI-based removal methods and composite attacks. This robustness, coupled with the ability to achieve

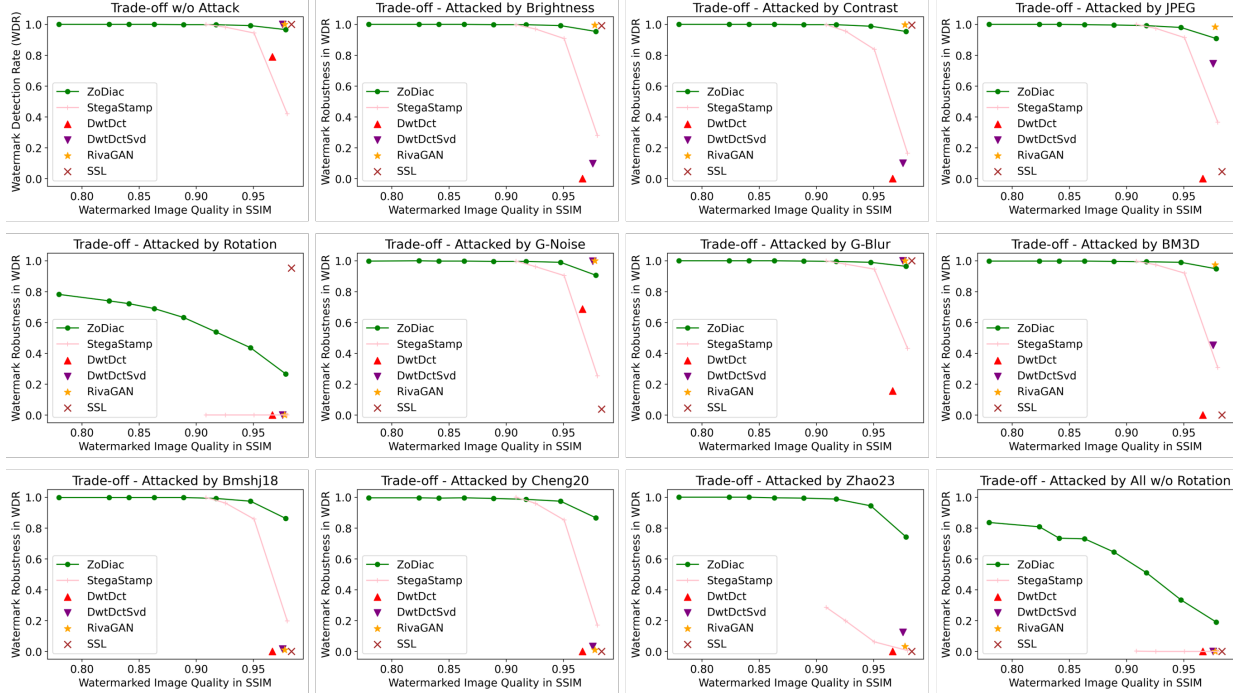


Figure 6: The trade-off between the watermarked image quality in terms of SSIM and the watermark robustness in terms of watermark detection rate (WDR) on **MS-COCO** dataset. The image quality is controlled by SSIM threshold $s^* \in [0.8, 0.98]$ with a step size of 0.03 as described in § 3.4 and the robustness is evaluated pre-attack and post-attack with different attack methods.

Table 7: The effects of varying detection thresholds $p^* \in \{0.90, 0.95, 0.99\}$ on watermark detection rate (WDR) and false positive rate (FPR). WDR is evaluated on watermarked images generated with SSIM threshold $s^* = 0.92$.

Detection Threshold p^*	FPR ↓	WDR ↑ before and after Attack			
		Pre-Attack	Post Attack		
			All	Rotation	Zhao23
COCO					
0.90	0.062	0.998	0.538	0.988	0.510
0.95	0.030	0.998	0.376	0.974	0.372
0.99	0.004	0.992	0.106	0.938	0.166
DiffusionDB					
0.90	0.050	1.000	0.558	0.988	0.548
0.95	0.018	1.000	0.356	0.952	0.418
0.99	0.004	0.998	0.130	0.902	0.174
WikiArt					
0.90	0.064	1.000	0.478	0.992	0.530
0.95	0.024	1.000	0.330	0.980	0.392
0.99	0.004	1.000	0.104	0.944	0.192

high-quality watermarked images, positions ZoDiac as a significant advancement in the field of image watermarking.

Limitation. The ZoDiac framework aligns with the paradigm of zero-bit watermarking (Furon, 2007), where the injector only hides a mark and the detector checks for its presence in the content. In other words, we cannot encode meaningful information such as binary numbers or a message as multi-bit watermarking. The constraint arises

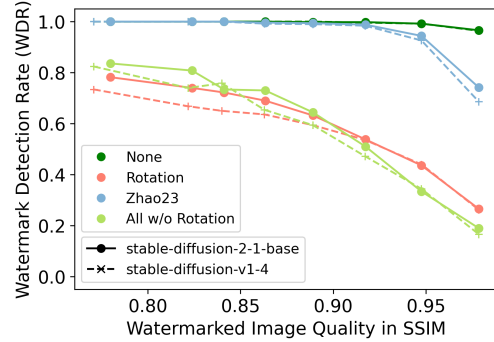


Figure 8: Comparisons between two pre-trained stable diffusion models, *stable-diffusion-2-1-base* and *stable-diffusion-v1-4*. The watermark detection rate is measured without attack or with three representative attacks, *Rotation*, *Zhao23*, and *All w/o Rotation*. Attack methods are marked by different colors. None represents “no attack”.

from the necessity to adhere to a Gaussian distribution in the initial latent vector of the diffusion model. Our future works tend to explore the possibility of hiding meaningful signals while preserving the robustness.

Table 9: Watermark detection rate (WDR) and false positive rate (FPR) when automatically correcting the image orientation before performing watermark detection for images under *Rotation* attack. Different correction step sizes and detection thresholds are evaluated.

MS-COCO, $s^* = 0.92$		Detection Threshold p^*	WDR	FPR
No Correction		0.9	0.538	0.062
		0.99	0.376	0.004
Correction Rotation Step Size	5	0.9	0.998	0.676
		0.99	0.992	0.034
	10	0.9	0.998	0.432
		0.99	0.992	0.016
	30	0.9	0.998	0.244
		0.99	0.992	0.014

Acknowledgments

This work is supported in part by the National Science Foundation under grants no. CCF-2210243, DMS-2220211, CNS-2224054, and CNS-2312396.

References

- Ballé, J., Minnen, D., Singh, S., Hwang, S. J., and Johnston, N. Variational image compression with a scale hyperprior. *arXiv preprint arXiv:1802.01436*, 2018.
- Bender, W., Gruhl, D., Morimoto, N., and Lu, A. Techniques for data hiding. *IBM systems journal*, 35(3.4):313–336, 1996.
- Bloom, J. A., Cox, I. J., Kalker, T., Linnartz, J.-P., Miller, M. L., and Traw, C. B. S. Copy protection for dvd video. *Proceedings of the IEEE*, 87(7):1267–1276, 1999.
- Boneh, D. and Shaw, J. Collusion-secure fingerprinting for digital data. *IEEE Transactions on Information Theory*, 44(5):1897–1905, 1998.
- Bors, A. G. and Pitas, I. Image watermarking using dct domain constraints. In *Proceedings of 3rd IEEE International Conference on Image Processing*, volume 3, pp. 231–234. IEEE, 1996.
- Chatterjee, A., Ghosal, S. K., and Sarkar, R. Lsb based steganography with ocr: an intelligent amalgamation. *Multimedia tools and applications*, 79(17-18):11747–11765, 2020.
- Cheng, Z., Sun, H., Takeuchi, M., and Katto, J. Learned image compression with discretized gaussian mixture likelihoods and attention modules. In *Proceedings of the IEEE/CVF conference on computer vision and pattern recognition*, pp. 7939–7948, 2020.
- Cox, I., Miller, M., Bloom, J., Fridrich, J., and Kalker, T. *Digital watermarking and steganography*. Morgan kaufmann, 2007.
- Craver, S. A., Memon, N. D., Yeo, B.-L., and Yeung, M. M. Can invisible watermarks resolve rightful ownerships? In *Storage and Retrieval for Image and Video Databases V*, volume 3022, pp. 310–321. SPIE, 1997.
- Cui, Y., Ren, J., Xu, H., He, P., Liu, H., Sun, L., and Tang, J. Diffusionshield: A watermark for copyright protection against generative diffusion models. *arXiv preprint arXiv:2306.04642*, 2023.
- Czolbe, S., Krause, O., Cox, I., and Igel, C. A loss function for generative neural networks based on watson’s perceptual model. *Advances in Neural Information Processing Systems*, 33:2051–2061, 2020.
- Dabov, K., Foi, A., Katkovnik, V., and Egiazarian, K. Image denoising by sparse 3-d transform-domain collaborative filtering. *IEEE Transactions on image processing*, 16(8):2080–2095, 2007.
- Dhariwal, P. and Nichol, A. Diffusion models beat gans on image synthesis. *Advances in neural information processing systems*, 34:8780–8794, 2021.
- Fernandez, P., Sablayrolles, A., Furon, T., Jégou, H., and Douze, M. Watermarking images in self-supervised latent spaces. In *ICASSP 2022-2022 IEEE International Conference on Acoustics, Speech and Signal Processing (ICASSP)*, pp. 3054–3058. IEEE, 2022.
- Fernandez, P., Couairon, G., Jégou, H., Douze, M., and Furon, T. The stable signature: Rooting watermarks in latent diffusion models. *arXiv preprint arXiv:2303.15435*, 2023.
- Furon, T. A constructive and unifying framework for zero-bit watermarking. *IEEE Transactions on Information Forensics and Security*, 2(2):149–163, 2007.
- Hosam, O. Attacking image watermarking and steganography-a survey. *International Journal of Information Technology and Computer Science*, 11(3):23–37, 2019.
- Huang, J., Luo, T., Li, L., Yang, G., Xu, H., and Chang, C.-C. Arwgan: Attention-guided robust image watermarking model based on gan. *IEEE Transactions on Instrumentation and Measurement*, 2023.
- Kingma, D. P. and Ba, J. Adam: A method for stochastic optimization. *arXiv preprint arXiv:1412.6980*, 2014.
- Kundur, D. and Hatzinakos, D. Digital watermarking using multiresolution wavelet decomposition. In *Proceedings of the 1998 IEEE International Conference on Acoustics, Speech and Signal Processing, ICASSP’98 (Cat. No. 98CH36181)*, volume 5, pp. 2969–2972. IEEE, 1998.
- Lee, J.-E., Seo, Y.-H., and Kim, D.-W. Convolutional neural network-based digital image watermarking adaptive to the resolution of image and watermark. *Applied Sciences*, 10(19):6854, 2020.
- Lin, T.-Y., Maire, M., Belongie, S., Hays, J., Perona, P., Ramanan, D., Dollár, P., and Zitnick, C. L. Microsoft coco: Common objects in context. In *Computer Vision—ECCV 2014: 13th European Conference, Zurich, Switzerland, September 6-12, 2014, Proceedings, Part V 13*, pp. 740–755. Springer, 2014.
- Luo, X., Zhan, R., Chang, H., Yang, F., and Milanfar, P. Distortion agnostic deep watermarking. In *Proceedings of the IEEE/CVF conference on computer vision and pattern recognition*, pp. 13548–13557, 2020.
- Patnaik, P. The non-central χ^2 -and f-distribution and their applications. *Biometrika*, 36(1/2):202–232, 1949.

- Phillips, F. and Mackintosh, B. Wiki art gallery, inc.: A case for critical thinking. *Issues in Accounting Education*, 26(3): 593–608, 2011.
- Ramesh, A., Dhariwal, P., Nichol, A., Chu, C., and Chen, M. Hierarchical text-conditional image generation with clip latents. *arXiv preprint arXiv:2204.06125*, 1(2):3, 2022.
- Rombach, R., Blattmann, A., Lorenz, D., Esser, P., and Ommer, B. High-resolution image synthesis with latent diffusion models. In *Proceedings of the IEEE/CVF conference on computer vision and pattern recognition*, pp. 10684–10695, 2022.
- Saharia, C., Chan, W., Saxena, S., Li, L., Whang, J., Denton, E. L., Ghasemipour, K., Gontijo Lopes, R., Karagol Ayan, B., Salimans, T., et al. Photorealistic text-to-image diffusion models with deep language understanding. *Advances in Neural Information Processing Systems*, 35:36479–36494, 2022.
- Sohl-Dickstein, J., Weiss, E., Maheswaranathan, N., and Ganguli, S. Deep unsupervised learning using nonequilibrium thermodynamics. In *International conference on machine learning*, pp. 2256–2265. PMLR, 2015.
- Solachidis, V. and Pitas, L. Circularly symmetric watermark embedding in 2-d dft domain. *IEEE transactions on image processing*, 10(11):1741–1753, 2001.
- Song, J., Meng, C., and Ermon, S. Denoising diffusion implicit models. *arXiv preprint arXiv:2010.02502*, 2020.
- Subhedar, M. S. and Mankar, V. H. Secure image steganography using framelet transform and bidiagonal svd. *Multimedia Tools and Applications*, 79:1865–1886, 2020.
- Tancik, M., Mildenhall, B., and Ng, R. Stegastamp: Invisible hyperlinks in physical photographs. In *Proceedings of the IEEE/CVF conference on computer vision and pattern recognition*, pp. 2117–2126, 2020.
- Tirkel, A. Z., Rankin, G., Van Schyndel, R., Ho, W., Mee, N., and Osborne, C. F. Electronic watermark. *Digital Image Computing, Technology and Applications (DICTA'93)*, pp. 666–673, 1993.
- Urvoy, M., Goudia, D., and Atrousseau, F. Perceptual dft watermarking with improved detection and robustness to geometrical distortions. *IEEE Transactions on Information Forensics and Security*, 9(7):1108–1119, 2014.
- Wan, W., Wang, J., Zhang, Y., Li, J., Yu, H., and Sun, J. A comprehensive survey on robust image watermarking. *Neurocomputing*, 488:226–247, 2022.
- Wang, Z., Bovik, A. C., Sheikh, H. R., and Simoncelli, E. P. Image quality assessment: from error visibility to structural similarity. *IEEE transactions on image processing*, 13(4):600–612, 2004.
- Wang, Z., Chen, C., Liu, Y., Lyu, L., Metaxas, D., and Ma, S. How to detect unauthorized data usages in text-to-image diffusion models. *arXiv preprint arXiv:2307.03108*, 2023.
- Wang, Z. J., Montoya, E., Munechika, D., Yang, H., Hoover, B., and Chau, D. H. Diffusiondb: A large-scale prompt gallery dataset for text-to-image generative models. *arXiv preprint arXiv:2210.14896*, 2022.
- Wen, Y., Kirchenbauer, J., Geiping, J., and Goldstein, T. Tree-rings watermarks: Invisible fingerprints for diffusion images. In *Thirty-seventh Conference on Neural Information Processing Systems*, 2023.
- Wolfgang, R. B. and Delp, E. J. A watermark for digital images. In *Proceedings of 3rd IEEE International Conference on Image Processing*, volume 3, pp. 219–222. IEEE, 1996.
- Xia, X.-G., Boncelet, C. G., and Arce, G. R. Wavelet transform based watermark for digital images. *Optics Express*, 3(12): 497–511, 1998.
- Zeng, Y., Zhou, M., Xue, Y., and Patel, V. M. Securing deep generative models with universal adversarial signature. *arXiv preprint arXiv:2305.16310*, 2023.
- Zhang, K., Zuo, W., Chen, Y., Meng, D., and Zhang, L. Beyond a gaussian denoiser: Residual learning of deep cnn for image denoising. *IEEE transactions on image processing*, 26(7):3142–3155, 2017.
- Zhang, K. A., Cuesta-Infante, A., Xu, L., and Veeramachaneni, K. Steganogan: High capacity image steganography with gans. *arXiv preprint arXiv:1901.03892*, 2019a.
- Zhang, K. A., Xu, L., Cuesta-Infante, A., and Veeramachaneni, K. Robust invisible video watermarking with attention. *arXiv preprint arXiv:1909.01285*, 2019b.
- Zhang, R., Isola, P., Efros, A. A., Shechtman, E., and Wang, O. The unreasonable effectiveness of deep features as a perceptual metric. In *Proceedings of the IEEE conference on computer vision and pattern recognition*, pp. 586–595, 2018.
- Zhao, H., Gallo, O., Frosio, I., and Kautz, J. Loss functions for image restoration with neural networks. *IEEE Transactions on computational imaging*, 3(1):47–57, 2016.
- Zhao, X., Zhang, K., Wang, Y.-X., and Li, L. Generative autoencoders as watermark attackers: Analyses of vulnerabilities and threats. *arXiv preprint arXiv:2306.01953*, 2023a.
- Zhao, Y., Pang, T., Du, C., Yang, X., Cheung, N.-M., and Lin, M. A recipe for watermarking diffusion models. *arXiv preprint arXiv:2303.10137*, 2023b.
- Zhu, J., Kaplan, R., Johnson, J., and Fei-Fei, L. Hidden: Hiding data with deep networks. In *Proceedings of the European conference on computer vision (ECCV)*, pp. 657–672, 2018.

Appendix

A. Ablation Study Continued

Trade-off Between Image Quality and Watermark Robustness. Figure 10 and 11 show the trade-off curves on the DiffusionDB and the WikiArt dataset respectively. The two figures plot the watermarked image quality in SSIM (x-axis) against the watermark detection rate (y-axis) subject to various attack scenarios. ZoDiac’s image quality is adjusted by SSIM thresholds $s^* \in [0.8, 0.98]$ with a step size of 0.03.

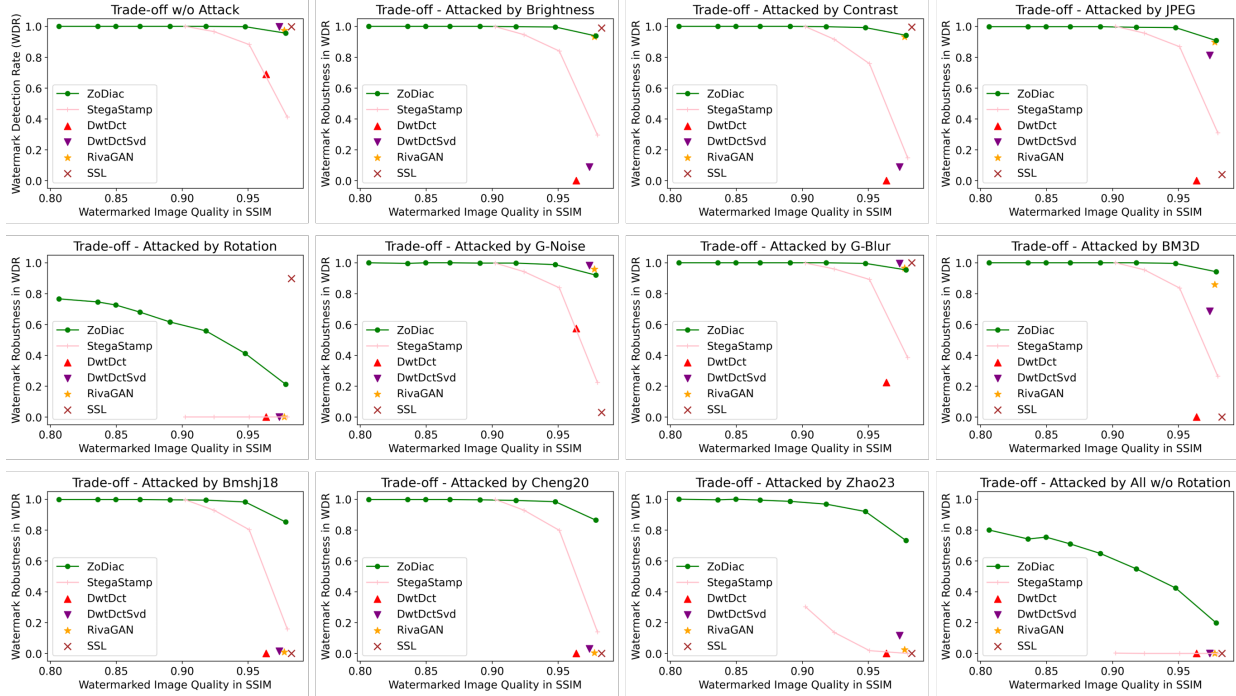


Figure 10: The trade-off between the watermarked image quality in terms of SSIM and the watermark robustness in terms of watermark detection rate (WDR) on **DiffusionDB** dataset. The image quality is controlled by SSIM threshold $s^* \in [0.8 : 0.98 : 0.03]$ in Section 3.4 and the robustness is evaluated with different attack methods.

WDR and FPR under Different Detection Threshold. Table 12 illustrates the effects of detection thresholds $p^* \in \{0.90, 0.95, 0.99\}$ on WDR and FPR. WDR is evaluated on watermarked images generated with SSIM threshold $s^* = 0.92$. Results for pre-attack and post-attack under all kinds of attacks are provided and WDR above 0.98 are highlighted by gray cells. As expected, a higher p^* usually corresponds to lower rates of both WDR and FPR. Specifically, under most attack conditions except *Rotation* and *All w/o Rotation*, WDR exhibits a marginal decline along with the increased p^* .

Flexibility Across Different Backbone Models. Figure 13 illustrates the watermarking performance comparisons between two pre-trained stable diffusion models, *stable-diffusion-2-1-base* and *stable-diffusion-v1-4*. The trade-off curves between the watermarked image quality and the watermark detection rate with and without attack are provided. Overall, the two backbone models exhibit similar watermarking performance.

B. Visual Examples

Figure 14 shows some invisible watermarking examples from each dataset. ZoDiac does not cause visible loss to image quality.

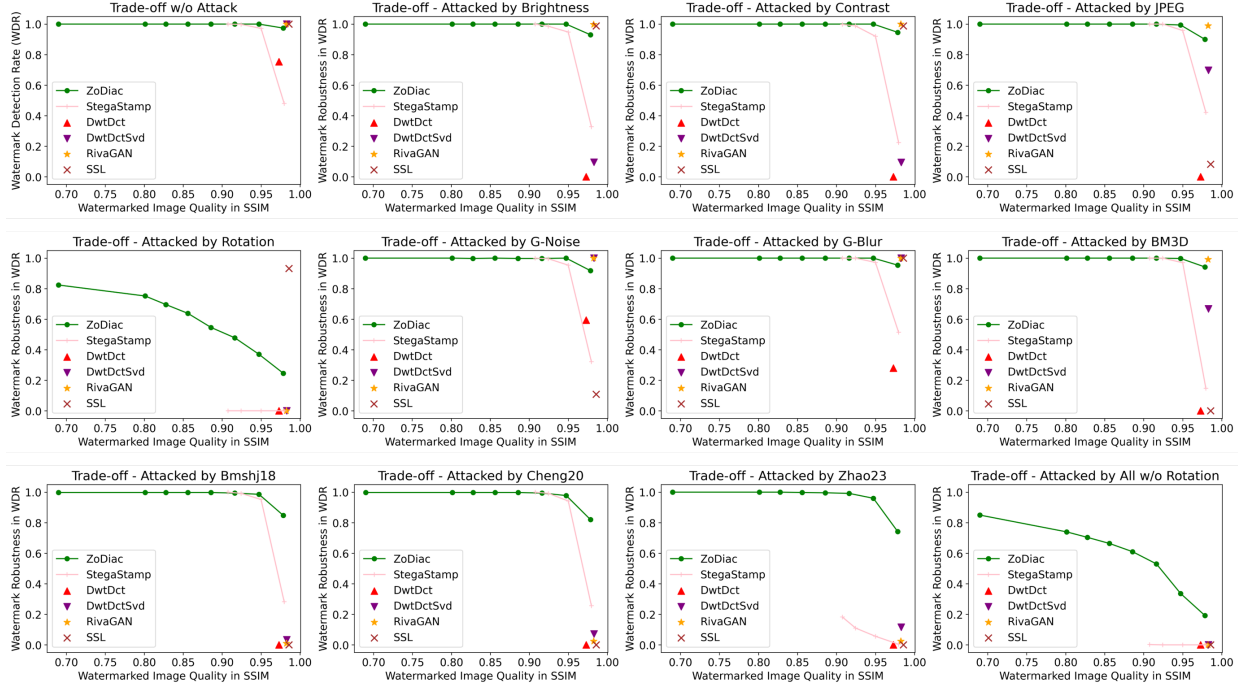


Figure 11: The trade-off between the watermarked image quality and the watermark robustness on **WikiArt** dataset similar to Figure 10.

Table 12: The effects of varying detection thresholds $p^* \in \{0.90, 0.95, 0.99\}$ on watermark detection rate (WDR) and false positive rate (FPR). WDR is evaluated on watermarked images generated with SSIM threshold $s^* = 0.92$. Results for pre-attack and post-attack under all attacks are provided.

Detection Threshold p^*	FPR ↓	Watermark Detection Rate (WDR) ↑ before and after Attacking												
		Pre-Attack	Post-Attack											
			Brightness	Contrast	JPEG	Rotation	G-Noise	G-Blur	BM3D	Bmshj18	Cheng20	Zhao23	All	All w/o Rotation
COCO														
0.90	0.062	0.998	0.998	0.998	0.992	0.538	0.996	0.996	0.994	0.992	0.986	0.988	0.072	0.510
0.95	0.030	0.998	0.996	0.998	0.992	0.376	0.996	0.996	0.994	0.986	0.978	0.974	0.028	0.372
0.99	0.004	0.992	0.990	0.990	0.978	0.106	0.984	0.988	0.988	0.960	0.954	0.938	0.000	0.166
DiffusionDB														
0.90	0.050	1.000	0.998	0.998	0.994	0.558	0.998	1.000	1.000	0.994	0.992	0.988	0.086	0.548
0.95	0.018	1.000	0.998	0.996	0.994	0.356	0.994	1.000	1.000	0.992	0.988	0.952	0.028	0.418
0.99	0.004	0.998	0.992	0.99	0.982	0.130	0.990	1.000	0.994	0.974	0.984	0.902	0.006	0.174
WikiArt														
0.90	0.064	1.000	1.000	1.000	1.000	0.478	0.998	1.000	1.000	0.994	0.994	0.992	0.082	0.530
0.95	0.024	1.000	1.000	1.000	0.998	0.330	0.996	1.000	0.998	0.994	0.990	0.980	0.032	0.392
0.99	0.004	1.000	1.000	1.000	0.992	0.104	0.994	1.000	0.998	0.980	0.964	0.944	0.002	0.192

Robust Image Watermarking using Stable Diffusion

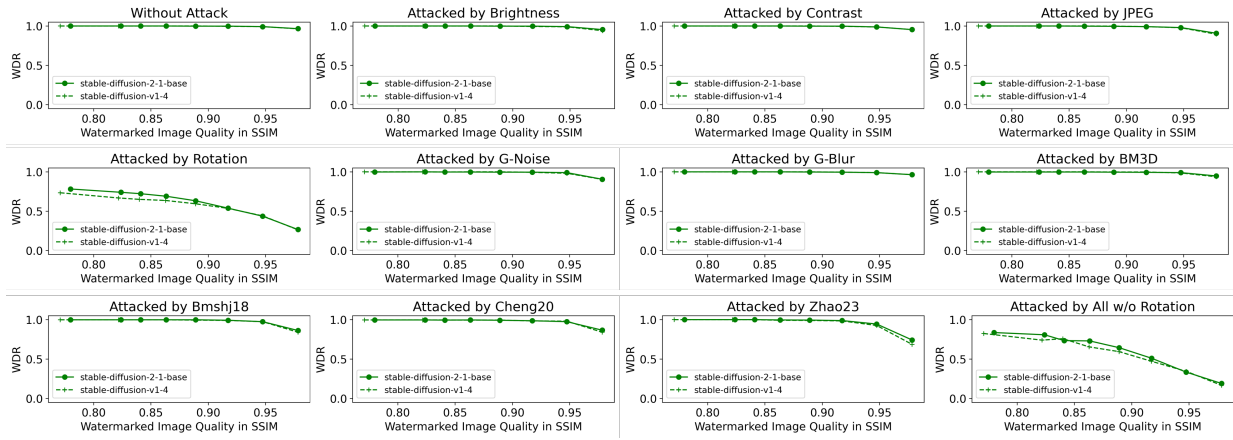


Figure 13: The watermarking performance comparisons between two pre-trained stable diffusion models, *stable-diffusion-2-1-base* and *stable-diffusion-v1-4*. The trade-off curves between the watermarked image quality and the watermark detection rate with and without attack are provided.



Figure 14: Examples of different invisible watermarking methods. The top two rows show real photos from the MS-COCO dataset, the next two rows show AI-generated content from DiffusionDB, and the last two rows are artworks from WikiArt. The SSIM threshold for ZoDiac is 0.92 for these examples.